



VICTORIA UNIVERSITY
MELBOURNE AUSTRALIA

System Identification and Robust Control of Multi-Input Multi-Output Active Magnetic Bearing Systems

This is the In Press version of the following publication

Noshadi, Amin, Shi, Juan, Lee, Wee, Shi, Peng and Kalam, Akhtar (2015)
System Identification and Robust Control of Multi-Input Multi-Output Active
Magnetic Bearing Systems. IEEE Transactions on Control Systems
Technology (99). ISSN 1063-6536 (In Press)

The publisher's official version can be found at
[http://ieeexplore.ieee.org/xpl/articleDetails.jsp?
arnumber=7294670&refinements=4224890905&filter=AND\(p_IS_Number:4389040\)](http://ieeexplore.ieee.org/xpl/articleDetails.jsp?arnumber=7294670&refinements=4224890905&filter=AND(p_IS_Number:4389040))
Note that access to this version may require subscription.

Downloaded from VU Research Repository <https://vuir.vu.edu.au/29781/>

System Identification and Robust Control of Multi-Input Multi-Output Active Magnetic Bearing Systems

Amin Noshadi, *Student Member, IEEE*, Juan Shi, *Member, IEEE*, Wee Sit Lee, *Member, IEEE*, Peng Shi, *Fellow, IEEE*, and Akhtar Kalam, *Senior Member, IEEE*

Abstract—This paper studies the system identification and robust control of a multi-input multi-output (MIMO) active magnetic bearing (AMB) system. The AMB system under study is open-loop unstable, and the presence of right-half plane zeros and the rotor flexible modes bring additional degrees of difficulty to the control design of such a system. Firstly, a closed-loop system identification is performed by using frequency-domain response data of the system. Genetic Algorithm-based Weighted Least Squares method is employed to obtain the best frequency-weighted model of the system. As the cross-coupling channels have negligible gains in the low-frequency region, it is assumed that the system can be diagonalized. This allows the analysis of the system as a family of low-order single-input single-output (SISO) subsystems. On the other hand, the effects caused by the coupling channels become more significant at higher frequencies. Therefore, a similar method is used to obtain a high-order MIMO model of the system by including the cross-coupling effects. Next, SISO H_∞ controllers and lead-lag type compensators are designed on the basis of the SISO models of the systems. To strive for a better performance, MIMO H_2 and H_∞ optimal controllers are synthesized on the basis of the MIMO model of the system. Extensive experimental studies are conducted on the performance of the designed SISO and MIMO controllers in real-time by taking into consideration both constant disturbances while the rotor is stationary, as well as sinusoidal disturbances caused by the centrifugal forces and the rotor mass-imbalance while the rotor is in rotation. Unlike the recently published works, it is shown that the accurate modeling of the system being controlled is the key to successful design of high-performance *stable* controllers that not only guarantee the internal stability of the system-controller interconnection, but also no further modifications are required before the real-time implementation of the designed controllers.

Index Terms—Active Magnetic Bearing Systems, Frequency-domain System Identification, Genetic Algorithm, Robust Control, H_2 Control, H_∞ Control

I. INTRODUCTION

In recent years, active magnetic bearing systems (AMBs) have attracted the attention of researchers as suitable replacements for conventional mechanical and hydrostatic bearings. AMBs can provide contactless suspension of the rotor by attractive forces produced by electromagnets. AMBs have

numerous advantages over their mechanical and hydrostatic counterparts. The primary advantage of AMBs is their extremely low frictional properties that allow efficient operations at high speeds [1]. AMBs can be utilized in many industrial applications where fast and precise operations are desired, such as linear induction motors, turbo-molecular vacuum pumps, artificial hearts, and gas-turbine engines [2]–[4]. In [5], a novel motor with a magnetically levitated rotor is designed, and its dynamic characteristics are simulated. The proposed motor is shown to have successfully achieved five degrees-of-freedom active control. The work in [6] studies the active surge control of a centrifugal compressor, where thrust active magnetic bearings (AMB) are employed. The results demonstrate the potential application of AMB-based compressor surge controllers. In [7], an AMB is applied as an actuator to guarantee chatter-free cutting operations in high-speed milling processes. A μ -synthesis approach is proposed for the robust stabilization of the fast milling process while minimizing the control efforts. Reference [8] investigates the application of active radial magnetic bearings for agile satellite systems. As a result, the control current and the associated power losses are considerably reduced. With the growing interest in the applications of fast and precise AMBs, there is a demand for developing advanced controllers that ensure robust performance of such systems in the presence of unmodeled dynamics and unknown external disturbances [9]–[12]. Although several works can be found on the analytical modeling and simulation of robust controllers on AMBs [13]–[16], system identification and real-time robust control of AMBs is a relatively recent development [17]–[26]. However, the results presented in the recent works have many shortcomings to consider this problem as solved. This gives reasonable motivations to address the current gaps between the theory and the challenges involved in real-time application of robust controllers on AMB systems. In the sequel, some of the shortcomings in the recent works are discussed in more details.

The work in [18] reports a single-input single-output (SISO) modeling and real-time implementation of H_∞ controller of an AMB system. An SISO controller is designed on the basis of the second-order model of the electromagnets. While low-bandwidth and hence low-performance controllers can always be designed on the basis of a low-order model of the system for stabilization purposes, the effects of the rotor resonant (flexible) modes, dynamic mass-imbalance, and centrifugal forces in high speeds could lead to system instability. In order

Amin Noshadi, Juan Shi, Wee Sit Lee, Peng Shi, and Akhtar Kalam are with the College of Engineering and Science, Victoria University, Melbourne, VIC 8001, Australia. e-mails: Amin.Noshadi@live.vu.edu.au, Juan.Shi@vu.edu.au, WeeSit.Lee@vu.edu.au, Peng.Shi@vu.edu.au, Akhtar.Kalam@vu.edu.au

Peng Shi is also with the School of Electrical and Electronic Engineering, The University of Adelaide, Adelaide, SA 5005, Australia; and the College of Automation, Harbin Engineering University, Harbin, China

Manuscript received ...; revised ...

to improve the performance of the system, it is necessary to find an accurate model of the system that captures the high-frequency dynamics precisely. The difficulties that may arise when a high-order model is used to design a robust controller can be seen in the recently published works. For instance, the frequency-domain results presented in [19] clearly show that the synthesized controllers fail to reject the effects caused by the high-frequency resonant (flexible) modes of the rotor. It is dangerous to implement such non-robust controllers on the system, as it could lead to system instability. To alleviate the problem, the work in [20] suggests to manually add additional notch filters to the controllers to ensure that the resonant modes of the rotor are not excited. However, this may unnecessarily increase the order of the controllers. More recently, the MIMO identification and H_∞ control synthesis of AMBs are investigated in [21], [22]. Firstly, a high-order MIMO model of the system, including the cross-couplings between all inputs and outputs is obtained from the frequency-domain response data of the system. Next, the identified model is used to synthesize the MIMO H_∞ controllers. Interestingly, all the synthesized controllers are found to be *unstable* and impossible to implement on the actual system. The fact that the synthesized *unstable* controllers fail to stabilize the system implies that the identified model may not represent the characteristics of the actual system being controlled. However, the authors proceed to implement the unstable controllers by first stabilizing the system using the low-performance *stable* controllers that are synthesized on the basis of a low-order model of the system, and gradually switching to the unstable controllers (in a time-span of five seconds). The successful switching between the controllers depends highly on the slow transition between the stable and unstable controllers. It should also be noted that the order of the MIMO H_∞ controllers are usually very high, and the presented Youla parameterization of the switching controllers further increases the order of the final controllers. This approach is not only impractical in the industrial applications, but also it is challenging to implement such excessively high-order controllers in real-time.

Synthesizing *unstable* H_∞ controllers that are not implementable on the system directly is not a trivial issue, and it may occur in the control synthesis of systems other than AMBs. The authors in [21], [22] claim that synthesizing unstable controllers is not a surprise, as the H_∞ synthesis algorithms tend to cancel the right-half plane (RHP) complex-conjugate zeros in the model of AMBs with RHP poles in the controller. To the best of our knowledge, there are several examples that the synthesized controllers include RHP poles, because the system model does not possess the parity interlacing property (PIP) [27], [28]. It is important to note that the PIP condition only applies to the poles and zeros on the real axis. Therefore, regardless of the location of the complex-conjugate poles and zeros in the model, as long as the PIP conditions are satisfied (which is the case for AMBs), there should exist *stable* controllers that guarantee the internal stability of the plant-controller interconnection, and no switching controllers are required. It is also emphasized in [27] that unstable controllers should only be used in special circumstances where stabilization with stable controllers is

infeasible, and should be avoided at all cost.

This paper investigates both SISO and MIMO modeling and robust control of an AMB laboratory experimental system. It is shown that the proper modeling of the system will result in *stable* high-performance controllers that can be implemented on the system directly and safely, without any additional modification or switching between the controllers. It should be further noted that the main aim of this paper is to obtain linear (SISO and MIMO) models of the AMB system and design high-performance linear (SISO and MIMO) controllers on the basis of the identified models. This allows us to make a fair comparison between the performance of the designed SISO and MIMO linear controllers and the analog on-board controllers. Moreover, the results can be compared with the recent works on the robust control of AMB systems. If nonlinear controllers were to be designed, nonlinear model of the system could be obtained and this was beyond the scope of this paper [29], [30]. The remaining of this paper is organized as follows. In Section II, frequency response data of the system are collected for the closed-loop system identification. The SISO and MIMO models of the system are obtained by employing the proposed Genetic Algorithm-based Weighted Least Squares (GA-WLS) algorithm. The advantage of obtaining the SISO models is studied in Section III, where low-order SISO H_∞ optimal controllers and conventional lead-lag type compensators can be designed on the basis of the identified SISO models, and their performance can be compared with the analog on-board controllers. In order to strive for a better performance, MIMO H_2 and H_∞ optimal controllers are designed on the basis of the identified MIMO model of the system in Section IV. Comprehensive experimental studies are conducted in Section V on the performance of the designed SISO and MIMO controllers in real-time while the rotor is stationary in the presence of constant disturbances, as well as while the rotor is in rotation at several speeds.

II. AMB SYSTEM DESCRIPTION AND MODEL IDENTIFICATION

The laboratory experimental AMB system is shown in Fig. 1. The system includes a rotor shaft, four pairs of horseshoe electromagnets (two pairs at each end), an air turbine driven by compressed air, four hall-effect sensors, four linear current-amplifiers, and four analog on-board controllers. The rotor is levitated with magnetic forces provided by the electromagnets, and the rotational speed of the rotor shaft can reach up to 10000 *rpm*. The rotor shaft has four degrees of freedom (4DOF) which are labeled as channels $Y_1 - Y_4$ in Fig. 1. Channels Y_1 and Y_2 correspond to the horizontal and vertical displacements of the rotor at one end. Whereas, channels Y_3 and Y_4 correspond to the horizontal and vertical displacements of the rotor at the other end of the system, respectively. A digital signal processing card (DS1104) [31] is used for the data acquisition and real-time implementation of the control algorithms.

AMBs are inherently open-loop unstable and hence closed-loop system identification must be performed instead of more common open-loop identification techniques [32], [33]. Fig. 2

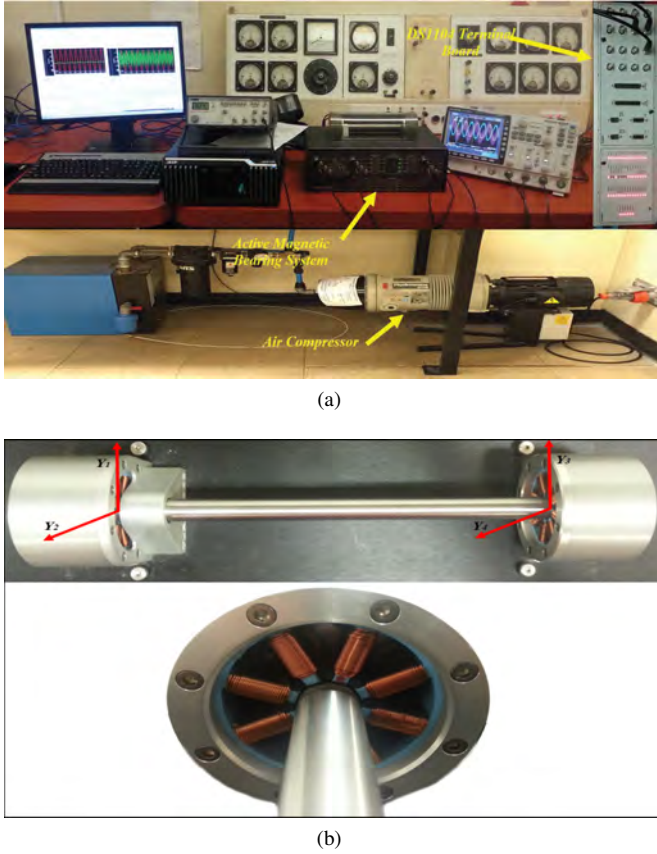


Fig. 1. Active magnetic bearing (AMB) system.

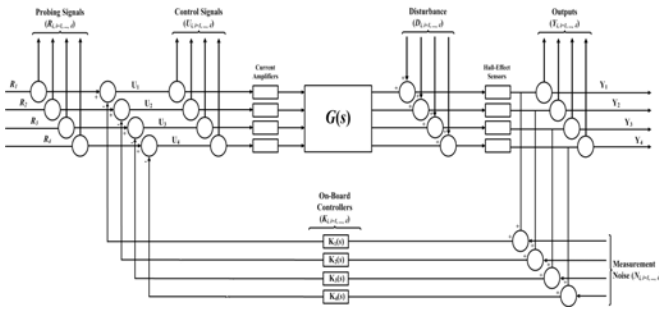


Fig. 2. Closed-loop system identification.

shows the block diagram of the setup that is used to collect the required data for the system identification stage. The data are taken while the rotor is stationary and stabilized with the four analog on-board controllers under the assumption that no disturbance is acting on the system.

A control-relevant system identification procedure on the AMB system is described here. Assuming that the closed-loop system is stable, and it is not subject to any external disturbances, the relationship between the plant outputs $Y = [Y_1, Y_2, Y_3, Y_4]^T$, the probing signals $R = [R_1, R_2, R_3, R_4]^T$, and the measurement noise $N = [N_1, N_2, N_3, N_4]^T$ is given in (1) (see Fig. 2).

$$Y(s) = \left(I + G(s)K(s) \right)^{-1} G(s)R(s) + \left(I + G(s)K(s) \right)^{-1} G(s)K(s)N(s) \quad (1)$$

Similarly, the relationship between the control signals $U = [U_1, U_2, U_3, U_4]^T$, the probing signals $R = [R_1, R_2, R_3, R_4]^T$, and the measurement noise $N = [N_1, N_2, N_3, N_4]^T$ can be obtained as in (2).

$$U(s) = \left(I + K(s)G(s) \right)^{-1} R(s) - \left(I + K(s)G(s) \right)^{-1} K(s)N(s) \quad (2)$$

Since the probing signals R and the measurement noise (with zero mean) N are uncorrelated, the transfer functions between the system outputs Y and the probing signals R can be obtained as in (3). For matrices of appropriate dimensions, (3) should follow the push-through rule:

$$T_{YR}(s) \approx \left(I + G(s)K(s) \right)^{-1} G(s) = G(s) \left(I + K(s)G(s) \right)^{-1} \quad (3)$$

Similarly, the transfer functions between the control signals U and the probing signals R can be simplified as in (4):

$$T_{UR}(s) \approx \left(I + K(s)G(s) \right)^{-1} \quad (4)$$

By using (3) and (4), the open-loop unstable SISO transfer functions of the system can be estimated from the closed-loop system identification as:

$$G(s) = T_{YR}(s)T_{UR}(s)^{-1} \quad (5)$$

Chirp signals are employed as the probing signals to the system for the purpose of collecting frequency response data. The initial frequency, target time, and the frequency at the target time of the chirp signals are chosen in such a way that the frequency does not increase too fast, so that the system has enough time to attain its steady-state response. In order not to overly excite the resonant frequencies, several sets of measurements have to be taken, each one within a certain range of frequency and amplitude. The MIMO measurements are taken by sending chirp signals to the input channels R and collecting the control signals U and the system output responses Y . The time-domain response of the system is collected using the dSPACE ControlDesk software and then exported to MATLAB for Discrete Fourier Transform (DFT) analysis. The obtained frequency-domain response (magnitude) of the system is shown in Fig. 3. The diagonal terms in Fig. 3 represent the frequency response between the input and output of the same channel. The off-diagonal terms, on the other hand, represent the cross-coupling effects between different channels. It can be seen from Fig. 3 that the gain contribution of the off-diagonal terms is small in the low-frequency region, i.e., a DC gain of about -20 dB or less. Therefore, if low-order (low-complexity) controllers are to be designed for the system, the MIMO system can be treated as four SISO subsystems, and the model of each subsystem can be obtained individually.

The SISO models of the system can be represented as linear time-invariant transfer functions of the form:

$$G(s) = \frac{N(s)}{D(s)} \quad (6)$$

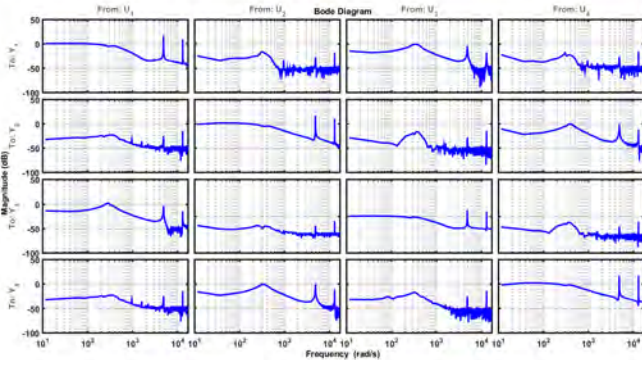


Fig. 3. Frequency-domain response data of the MIMO AMB system.

where,

$$N(s) = [n_0 + n_1(s) + n_2(s)^2 + \dots + n_k(s)^k], \quad \forall s = j\omega$$

$$D(s) = [1 + d_1(s) + d_2(s)^2 + \dots + d_l(s)^l], \quad \forall s = j\omega$$

In order to have a proper system, the order of the numerator (k) has to be less than or equal to the order of the denominator (l). From the DFT analysis of the input and output signals of the system at all experimental frequencies ($\omega_1, \omega_2, \dots, \omega_N$), a non-parametric model of the system can be obtained as $\hat{G}(j\omega)$. The operator $\hat{\cdot}$ is used because there are always unavoidable errors in the measurement. Since it is assumed that $\hat{G}(j\omega) = N(j\omega)/D(j\omega)$, we have:

$$D(j\omega)\hat{G}(j\omega) = N(j\omega) \quad (7)$$

The unknown coefficients (n_0, n_1, \dots, n_k), and (d_1, d_2, \dots, d_l) can be evaluated by minimizing the sum of squared of moduli of the errors between the frequency response of the fitted transfer function $N(s)/D(s)$ and the collected frequency response data $\hat{G}(j\omega)$ [34]:

$$J = \sum_{i=1}^N e_i^* e_i \quad (8)$$

where, $e_i = D(j\omega_i)\hat{G}(j\omega_i) - N(j\omega_i)$, and $*$ denotes complex-conjugate transpose. The term e_i can be expressed as:

$$e_i = \left[1 + d_1(j\omega_i) + \dots + d_l(j\omega_i)^l \right] \hat{G}(j\omega_i) - \left[n_0 + n_1(j\omega_i) + \dots + n_k(j\omega_i)^k \right] \quad (9)$$

or alternatively:

$$e_i = \hat{G}(j\omega_i) - \left[- (j\omega_i)\hat{G}(j\omega_i), \dots, -(j\omega_i)^l \hat{G}(j\omega_i), 1, j\omega_i, \dots, (j\omega_i)^k \right] \theta \quad (10)$$

where $\theta = [d_1, d_2, \dots, d_l, n_0, n_1, \dots, n_k]^T$ is a vector of unknown parameters. The cost function J can now be expressed as:

$$J = \sum_{i=1}^N e_i^* e_i = (Y - X\theta)^*(Y - X\theta) \quad (11)$$

where,

$$\theta = [d_1, d_2, \dots, d_l, n_0, n_1, \dots, n_k]^T$$

$$Y = [\hat{G}(j\omega_1), \hat{G}(j\omega_2), \dots, \hat{G}(j\omega_N)]^T$$

$$X = \begin{bmatrix} -j\omega_1 \hat{G}(j\omega_1) & \dots & -(j\omega_1)^l \hat{G}(j\omega_1) & 1 & j\omega_1 & \dots & (j\omega_1)^k \\ \vdots & & & & & & \vdots \\ -j\omega_N \hat{G}(j\omega_N) & \dots & -(j\omega_N)^l \hat{G}(j\omega_N) & 1 & j\omega_N & \dots & (j\omega_N)^k \end{bmatrix}$$

The cost function J as a function of θ can be minimized by differentiating J with respect to each unknown parameter in θ and setting the result to zero. The value of θ that minimizes J can be obtained as:

$$\theta = (X^* X)^{-1} (X^* Y) \quad (12)$$

In a standard least-squares problem, it is assumed that the collected response data are of equal quality and hence have a constant noise variance. However, if this assumption does not hold, the quality of the fitted model can be influenced by poor quality data. To improve the model at certain ranges of frequencies, one can use weighted least-squares where the frequency weighting is used to emphasize the frequencies of interest. The weighted least-squares minimizes the sum squared of the weighted error:

$$J = \sum_{i=0}^N w_i e_i^* e_i \quad (13)$$

The weights w_i determine how much each response value influences the final parameter estimates. Note that the weights w_i are positive definite and they are given as the diagonal elements of the weight matrix W :

$$W = \begin{bmatrix} w_1 & 0 & \dots & 0 \\ 0 & w_2 & \dots & 0 \\ \vdots & \vdots & \ddots & \vdots \\ 0 & 0 & \dots & w_N \end{bmatrix} \quad (14)$$

The unique solution to the weighted least-squares problem is in the form of (15):

$$\theta = (X^* W X)^{-1} (X^* W Y) \quad (15)$$

For the AMBs under study, the two flexible (resonant) modes of the rotor need to be modeled accurately, as they are within the bandwidth of the system. The problem with most of the available methods is that the algorithm finds an accurate model of the system in the low-frequency region, but fails to model the resonant modes. We aim to find a model of the system that is as simple as possible, and yet capable of capturing all the important characteristics of the plant. To overcome this problem, Genetic Algorithm (GA) [35]–[38] is employed to find the required frequency weightings (fictitious noise components) automatically, and perform an iterative re-weighted least squares algorithm. In this approach, GA generates a random vector of $w_i > 0$ to be the diagonal elements of the weight matrix W . Then, GA alters the weights

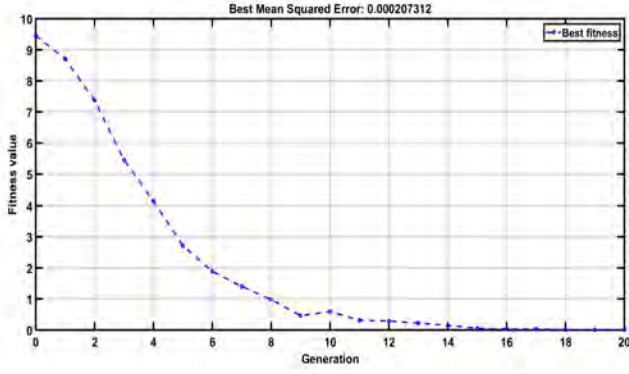


Fig. 4. Convergence of GA.

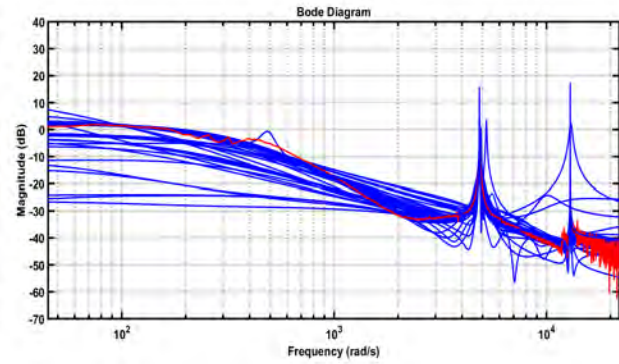


Fig. 5. A snapshot of GA optimization.

by changing the range and scaling factors in the vector w_i . The WLS is solved on the basis of the updated weight matrix, and the iteration continues until the minimum difference between the frequency response of the model and the experimental data and a predefined value is achieved (or the maximum number of iterations is reached). In order to scale up the errors around the two resonant modes, six variables are defined. These parameters are mainly the lower and upper frequency ranges of interest ($[\omega_{1-start}, \omega_{1-end}]$, and $[\omega_{2-start}, \omega_{2-end}]$), and their corresponding scaling factors (α and β) as shown in (16). The optimum value of (α and β) are to be found by the GA to heavily penalize the fitting error in a particular range of frequencies where the modeling accuracy is important.

$$w_i = \left[1, \dots, 1, \alpha\omega_{1-start}, \dots, \alpha\omega_{1-end}, 1, \dots, 1, \right. \\ \left. \beta\omega_{2-start}, \dots, \beta\omega_{2-end}, 1, \dots, 1 \right] \quad (16)$$

Figs. 4 and 5 show the convergence of GA and the effect of the frequency weighting on the explicit solution of the least-squares problem and hence on the frequency response of the modeled transfer function. It should be noted that the optimization process is only illustrated for the first channel, and relatively similar results are obtained for the other three channels.

It is important to note that the desired order of the model has to be assigned before the optimization process is initiated. Since the total order of four is required to model the two flexible (resonant) modes of the rotor, it can be deduced

that models with order less than five will fail to accurately model the behavior of the actual system. Therefore, a sixth-order model is chosen to ensure the accurate modeling of the system at the frequency ranges of interest. The obtained SISO models of all four channels using the proposed methods are compared with two common methods, namely, the prediction error method (PEM), and the numerical subspace state-space (N4SID) identification method in Fig. 6. The results show the effectiveness of the proposed method in the identification of systems that include both slow and fast dynamics. The resulting transfer functions of all four channels are presented in (17)-(20).

$$G_1(s) = \frac{-0.0054872(s+1.72 \times 10^4)(s-2075)}{(s+374.4)(s-310.2)} \\ \times \frac{(s^2+4240s+2.127 \times 10^7)(s^2+3305s+1.637 \times 10^8)}{(s^2+0.96s+2.344 \times 10^7)(s^2+0.37s+1.668 \times 10^8)} \quad (17)$$

$$G_2(s) = \frac{-0.0205(s+5699)(s-1588)}{(s+433.4)(s-233.4)} \\ \times \frac{(s^2+4168s+2.127 \times 10^7)(s^2+3140s+1.631 \times 10^8)}{(s^2+0.27s+2.307 \times 10^7)(s^2+0.3s+1.673 \times 10^8)} \quad (18)$$

$$G_3(s) = \frac{-0.01993(s+5178)(s-2135)}{(s+628.1)(s-215.5)} \\ \times \frac{(s^2+4083s+2.329 \times 10^7)(s^2+5183s+1.631 \times 10^8)}{(s^2+0.31s+2.399 \times 10^7)(s^2+0.35s+1.673 \times 10^8)} \quad (19)$$

$$G_4(s) = \frac{-0.04793(s+3912)(s-1189)}{(s+388.4)(s-246.7)} \\ \times \frac{(s^2+4022.66s+1.947 \times 10^7)(s^2+3743s+1.631 \times 10^8)}{(s^2+0.529s+2.3 \times 10^7)(s^2+0.726s+1.65 \times 10^8)} \quad (20)$$

The described approach for the SISO modeling of the system can be extended to estimate the MIMO model of the system (including the cross-coupling effects in Fig. 3), if a high-order MIMO controller is to be designed on the basis of the MIMO model of the system. Suppose that the model is represented in the state-space form (assuming that the feed-through term D is zero):

$$\dot{x}(t) = Ax(t) + Bu(t), \quad x \in R^n, \quad u \in R^k \\ y = Cx(t), \quad y \in R^m \quad (21)$$

It is assumed that the system has k inputs, m outputs, and n states. A transfer function representation of the system can be obtained as:

$$G(s) = C(sI - A)^{-1}B, \quad \forall s = j\omega \quad (22)$$

Similar to the SISO case, the vector of unknown parameters $\theta = [vec(A)^T, vec(B)^T, vec(C)^T]^T$ can be estimated by minimizing the weighted sum of the squared errors between the frequency response of the state-space model $G(s)$ and the experimental data at all experimental points $\hat{G}(j\omega)$:

$$J = \sum_{i=1}^N w_i \|\hat{G}(j\omega_i) - G(j\omega_i)\|^2 \quad (23)$$

Again, GA is utilized to obtain the best weighting vector that minimizes the cost function J over the unknown parameter vector θ . Note that a higher-order model is required to successfully describe the dynamics of the MIMO system including the cross-couplings. After some trials, an eighteenth-order state-space model of the system is found to have a fair

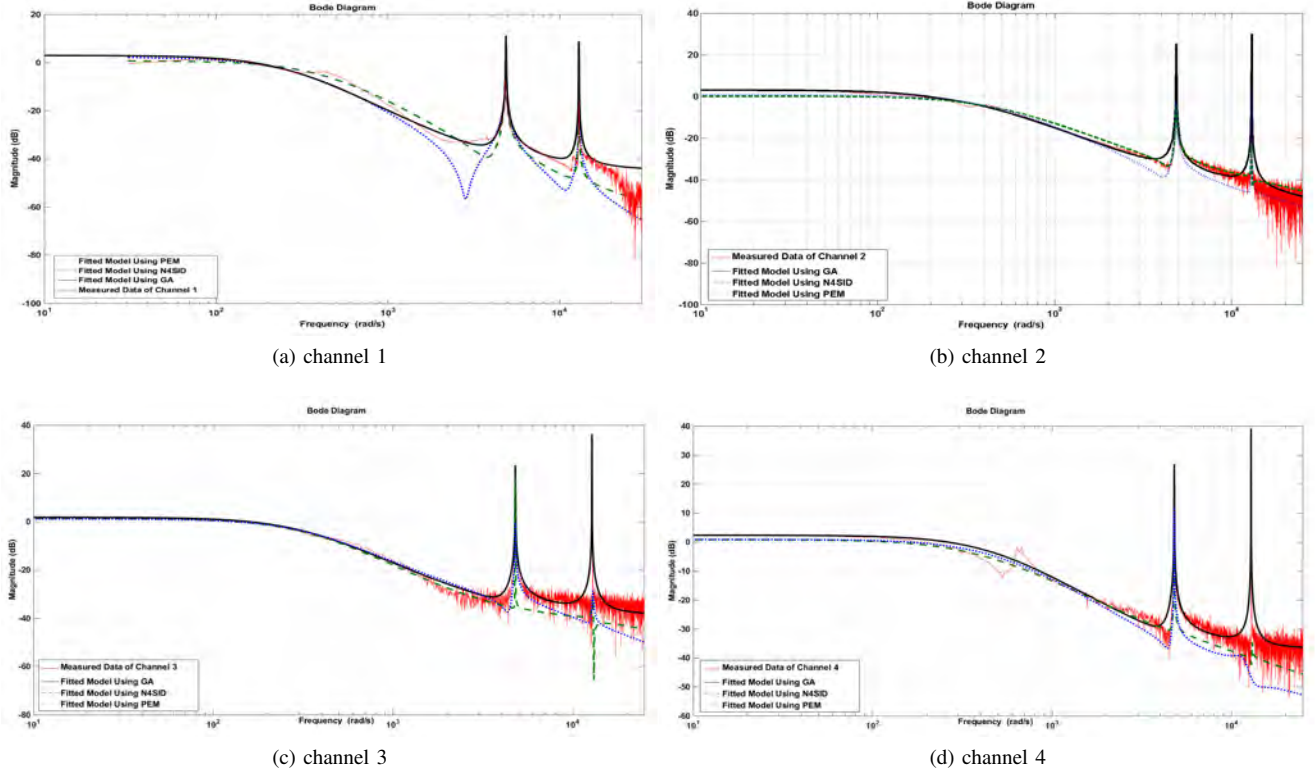


Fig. 6. Bode (magnitude) diagrams of the identified SISO models of the system using the presented algorithm, PEM, and N4SID.

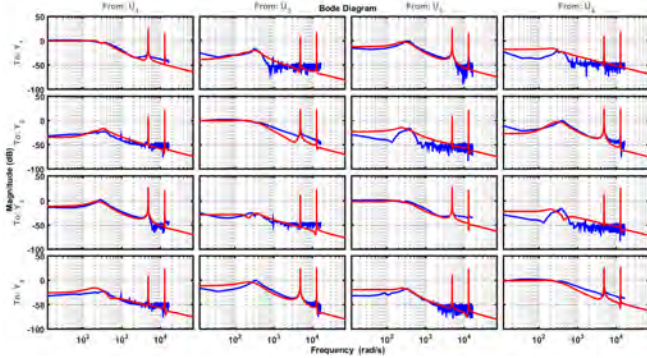


Fig. 7. The identified MIMO model of the system and the experimental frequency response data.

representation of the actual system dynamics. The frequency response of the MIMO model is shown in Fig. 7, and it is compared with the collected frequency-domain signals. The state-space representation of the obtained eighteenth-order MIMO model of the system is given in the Appendix, and it is used for the synthesis of the MIMO H_2 and H_∞ controllers.

III. SISO CONTROLLERS DESIGN

This section is devoted to the synthesis of controllers that are designed on the basis of the identified SISO models of the system. First, four SISO H_∞ optimal controllers are synthesized on the basis of the SISO models, and some useful remarks are given for the design of the weighting functions

required in the H_∞ synthesis procedure. To demonstrate the advantages of the H_∞ synthesis algorithms over the classical design methods, four lead-lag type compensators are also designed on the basis of the identified SISO models.

A. Mixed-Sensitivity H_∞ Controller Design

In a standard mixed-sensitivity H_∞ control problem, three weighting functions can be designed to shape the closed-loop behavior of the system (see Fig. 8). A weighting function $W_P(s)$ is designed to bound the closed-loop sensitivity function ($S(s) = (I + G(s)K(s))^{-1}$) to improve the steady-state error of the system, and ensure the rejection of low-frequency disturbances. Another weighting function $W_T(s)$ bounds the closed-loop complementary sensitivity function ($T(s) = G(s)K(s)(I + G(s)K(s))^{-1}$) to ensure the system robustness against model uncertainties and high-frequency measurement noise. Finally, $W_U(s)$ can be optionally designed to penalize the control signal to prevent the actuators saturation.

The requirements can be absorbed into a stacked H_∞ optimization problem, and the feedback system can be rearranged as a linear fractional transformation (LFT). The weighting functions ($W_P(s)$, $W_T(s)$, and $W_U(s)$) can be easily combined with the system and represented as a generalized (augmented) plant $P(s)$ [39]. The closed-loop transfer function between the generalized plant and the controller can be found as:

$$T := \mathcal{F}_l(P, K) = P_{11} + P_{12}K(I - P_{22}K)^{-1}P_{21} \quad (24)$$

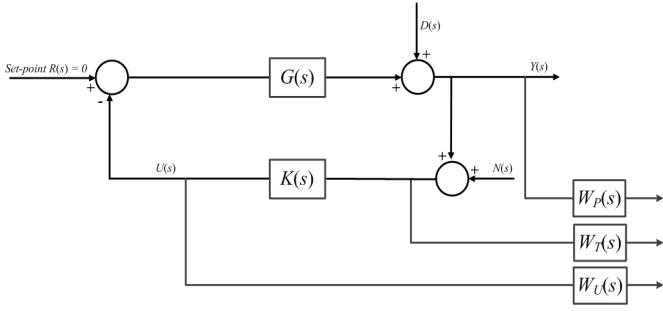


Fig. 8. Mixed S/T/KS sensitivity problem.

In (24), $\mathcal{F}_l(P, K)$ is the lower linear fractional transformation (LFT) of P with respect to K . Also, $P_{11} = [0, 0, W_P I]^T$, $P_{12} = [W_U I, W_T G, W_P G]^T$, $P_{21} = -I$, and $P_{22} = -G$. The H_∞ mixed-sensitivity optimization problem is to find a controller $K(s)$ which robustly stabilizes the system, and minimizes the H_∞ -norm of the closed-loop transfer function of the augmented plant $P(s)$.

$$\min_{K \text{ stabilizing}} \left\| \mathcal{F}_l(P, K) \right\|_\infty \quad (25)$$

where,

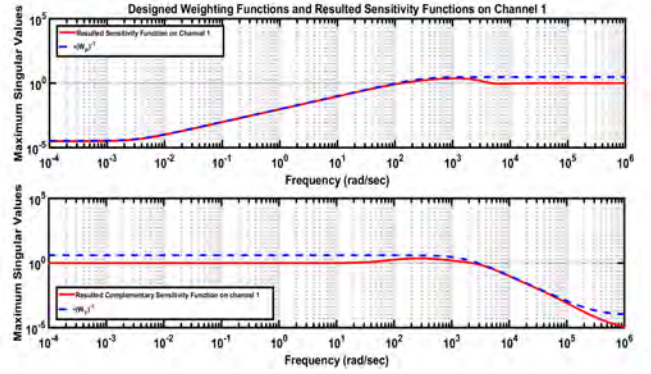
$$\left\| \mathcal{F}_l(P, K) \right\|_\infty = \left\| \begin{array}{c} W_P S \\ W_U K S \\ W_T T \end{array} \right\|_\infty \quad (26)$$

In recent years, H_∞ algorithms have become well-known methods to synthesize model-based controllers that satisfy a number of constraints and performance requirements expressed in the form of weights on the closed-loop sensitivity and complementary sensitivity functions. However, the successful design of these weights in H_∞ control problems is a non-trivial task primarily based on engineering intuition. As the AMB system under study is unstable and non-minimum phase, the successful design of weighting functions required in the synthesis of H_∞ controllers may become a challenging task. The presence of the flexible (resonant) modes of the rotor brings an additional degree of difficulty to the design of these weighting functions. In the sequel, some useful remarks concerning the design of H_∞ controllers for unstable non-minimum phase systems are given which could help in the design of the weighting functions.

Remark 1: Although it is desirable that $|S(j\omega)| \ll 1$, $\forall j\omega$ and $|T(j\omega)| \ll 1$, $\forall j\omega$, it is important to note that the presence of unstable poles/zeros increases the peak of sensitivity functions. It implies that the peak values of $S(s)$ and $T(s)$ exceed one, and this is unavoidable. For a system with RHP-zero ($s = z$) and RHP-pole ($s = p$), the sensitivity peaks can be evaluated as in (27) [40].

$$\|S\|_\infty > c, \|T\|_\infty > c, c = \frac{|z + p|}{|z - p|} \quad (27)$$

Remark 2: In the presence of RHP-pole ($s = p$), a high gain controller is required to stabilize the open-loop unstable system. However, it is impossible to employ large loop gain in the frequency range close to the location of RHP-zero ($s = z$)


 Fig. 9. Singular values of $S(s)$, $T(s)$, $1/W_P(s)$, and $1/W_T(s)$ of channel 1.

while maintaining stability. It implies that for a system with RHP poles and zeros, a closed-loop bandwidth of $2p < \omega_c < z$ is expected.

Remark 3: The peak values of the sensitivity functions (M_P and M_T) are very closely related to the gain and phase margins and hence the following conditions are very useful for the performance analysis of the system [40], [41]:

$$GM \geq \frac{M_P}{M_P - 1}, PM \geq 2 \arcsin\left(\frac{1}{2M_P}\right) (\text{rad}) \quad (28)$$

$$GM \geq \frac{M_T}{M_T - 1}, PM \geq 2 \arcsin\left(\frac{1}{2M_T}\right) (\text{rad}) \quad (29)$$

Following the given remarks, first-order performance weighting functions ($W_P(s)$) are designed to be the upper bounds on the closed-loop sensitivity functions. In (30), the integral action is replaced by a small number to avoid the numerical issues, and a closed-loop bandwidth of (0.3333×500) is desired. Furthermore, second-order ($W_T(s)$) weighting functions are chosen as the upper bounds on the complementary sensitivity functions. Note that choosing a second order $W_T(s)$ ensures the complete removal of the resonant frequencies at higher frequencies. Due to the page limitation, the designed weighting functions for the first channel are given in (30), and the resulting closed-loop sensitivity and complementary sensitivity functions ($S(s)$ and $T(s)$) are depicted in Fig. 9. However, similar weighting functions are designed for all four channels. Finally, the obtained continuous-time controllers for all four channels are given in (31)-(34). Since the models satisfy the PIP condition, the synthesized controllers are found to be *stable* and hence can be implemented on the system safely and reliably.

$$W_P(s) = \frac{0.3333(s + 500)}{(s + 0.00333)}, W_T(s) = \frac{10^4(s + 1500)^2}{(s + 3 \times 10^5)^2} \quad (30)$$

$$K_{1\infty} = \frac{7986.2(s + 3 \times 10^5)^2(s + 374.4)}{(s + 4.822 \times 10^5)(s + 1.717 \times 10^4)(s + 0.003333)} \frac{(s + 77.94)(s^2 + 0.96s + 2.344 \times 10^7)}{(s^2 + 5087s + 2.191 \times 10^7)(s^2 + 6429s + 2.328 \times 10^7)} \frac{(s^2 + 0.37s + 1.668 \times 10^8)}{(s^2 + 5297s + 1.637 \times 10^8)} \quad (31)$$

$$K_{2\infty} = \frac{923.21(s + 3 \times 10^5)^2(s + 433.4)}{(s + 4.822 \times 10^5)(s + 1.717 \times 10^4)(s + 0.003333)} \frac{(s + 71.86)(s^2 + 0.27s + 2.307 \times 10^7)}{(s^2 + 5755s + 2.002 \times 10^7)(s^2 + 5755s + 2.002 \times 10^7)} \frac{(s^2 + 0.37s + 1.673 \times 10^8)}{(s^2 + 5139s + 1.631 \times 10^8)} \quad (32)$$

$$K_{3\infty} = \frac{718.62(s + 3 \times 10^5)^2(s + 628.1)}{(s + 1.739 \times 10^5)(s + 5125)(s + 0.003333)} \frac{(s + 91.89)(s^2 + 0.031s + 2.344 \times 10^7)}{(s^2 + 6464s + 2.443 \times 10^7)(s^2 + 4983s + 2.136 \times 10^7)} \frac{(s^2 + 0.037s + 1.668 \times 10^8)}{(s^2 + 5139s + 1.637 \times 10^8)} \quad (33)$$

$$K_{4\infty} = \frac{1321(s + 388.4)(s + 50.52)}{(s + 6.884 \times 10^5)(s + 3892)(s + 0.003333)} \frac{(s^2 + 6.4 \times 10^5s + 1.024 \times 10^{11})(s^2 + 0.0529s + 2.3 \times 10^7)}{(s^2 + 4977s + 1.99 \times 10^7)(s^2 + 5473s + 2.134 \times 10^7)} \frac{(s^2 + 0.0726s + 1.65 \times 10^8)}{(s^2 + 4743s + 1.661 \times 10^8)} \quad (34)$$

B. Lead-Lag Type Compensator Design

In order to design SISO controllers using the classical methods, two notch filters need to be designed (for each channel) first to ensure that the resonant modes are not excited. The following structure is used for the notch filters:

$$N(s) = \frac{s^2 + \zeta b \omega_n s + \omega_n^2}{s^2 + b \omega_n s + \omega_n^2} \quad (35)$$

In (35), ω_n is the notch frequency, ζ is the damping ratio, and b is the bandwidth of the notch filter. After designing the required notch filters, a reduced-order SISO model can be obtained by removing the poles and zeros corresponding to the resonant modes from the model while keeping their DC gains in the reduced-order model. Next, a compensator can be designed on the basis of the reduced-order model of the system. PID controllers are very common in the industry. However, the presence of pure integrators can lead to integral windup problems. Therefore, a lead-lag compensator is preferred here and it can be designed on the basis of the reduced-order model:

$$K_{lead-lag} = K_{lead} K_{lag} \frac{(s + a)}{(s + \gamma a)} \frac{(s + \beta b)}{(s + b)}, \text{ with } \beta, \gamma > 1 \quad (36)$$

Finally, a second order low-pass filter is added to the compensator to increase the high-frequency roll-off rate, so that gain desensitization is secured in the high-frequency regions. For a fair comparison between the classically designed lead-lag compensators and the SISO H_∞ controllers, similar time- and frequency-domain requirements are used for the design of the lead-lag compensators. The final SISO lead-lag type compensators for all four channels are given in (37)-(40).

$$K_{lead-lag(1)} = \frac{1.0994 \times 10^{10}(s + 379.5)(s + 120)}{(s + 2.5 \times 10^4)^2(s + 3795)(s + 32.85)} \frac{(s^2 + 0.2449s + 2.344 \times 10^7)(s^2 + 0.1194s + 1.668 \times 10^8)}{(s^2 + 5421s + 2.344 \times 10^7)(s^2 + 3775s + 1.668 \times 10^8)} \quad (37)$$

$$K_{lead-lag(2)} = \frac{7.9158 \times 10^9(s + 406.7)(s + 120)}{(s + 2.5 \times 10^4)^2(s + 2927)(s + 32.85)} \frac{(s^2 + 0.0708s + 2.307 \times 10^7)(s^2 + 0.107s + 1.673 \times 10^8)}{(s^2 + 4955s + 2.307 \times 10^7)(s^2 + 3384s + 1.673 \times 10^8)} \quad (38)$$

$$K_{lead-lag(3)} = \frac{8.7532 \times 10^9(s + 459.8)(s + 132.2)}{(s + 2.5 \times 10^4)^2(s + 3310)(s + 21.06)} \frac{(s^2 + 4.165 \times 10^{-6}s + 2.344 \times 10^7)(s^2 + 5.214 \times 10^{-7}s + 1.668 \times 10^8)}{(s^2 + 4220s + 2.344 \times 10^7)(s^2 + 5214s + 1.668 \times 10^8)} \quad (39)$$

$$K_{lead-lag(4)} = \frac{6.6619 \times 10^9(s + 308.2)(s + 116.9)}{(s + 2.5 \times 10^4)^2(s + 3346)(s + 19.63)} \frac{(s^2 + 2.85 \times 10^{-4}s + 2.3 \times 10^7)(s^2 + 8.927 \times 10^{-7}s + 1.65 \times 10^8)}{(s^2 + 6466s + 2.3 \times 10^7)(s^2 + 8927s + 1.65 \times 10^8)} \quad (40)$$

IV. MIMO H_2 AND H_∞ CONTROLLERS

In order to investigate the effects of the cross-coupling channels on the overall performance of the system, MIMO H_2 and H_∞ optimal controllers are synthesized on the basis of the high-order MIMO model (given in the Appendix). Again, similar weighting functions are employed for the synthesis of the MIMO controllers (similar to (30)). This ensures that the conditions of all SISO and MIMO controllers are similar and hence the comparison between the performance of these controllers is fair, i.e.:

$$\mathbf{W}_P(s) = \text{diag}\{W_P(s), W_P(s), W_P(s), W_P(s)\},$$

$$\mathbf{W}_T(s) = \text{diag}\{W_T(s), W_T(s), W_T(s), W_T(s)\}$$

The MIMO diagonal weighting matrices ($\mathbf{W}_P(s)$, $\mathbf{W}_U(s)$, and $\mathbf{W}_T(s)$) are augmented with the MIMO model of the system, and the mixed-sensitivity H_2 and H_∞ optimization procedures are performed on the generalized plant, respectively. Note also that the standard mixed-sensitivity H_2 loop-shaping problem is to find a stabilizing controller K that minimizes the H_2 norm of the closed-loop system as in (41) [40], [42].

$$\min_{K \text{ stabilizing}} \left\| \begin{array}{c} \mathbf{W}_P S \\ \mathbf{W}_U K S \\ \mathbf{W}_T T \end{array} \right\|_2 \quad (41)$$

Fig. 10 shows the frequency response plot of the resulting closed-loop sensitivity and complementary sensitivity functions ($S(s)$ and $T(s)$) using the MIMO H_2 and H_∞ controllers. Since similar weighting functions are used for the synthesis of the H_2 and H_∞ controllers, similar performances are expected from the two controllers. However, the real-time experiments reveal some interesting results in the next section.

V. EXPERIMENTAL VALIDATION

To evaluate the performance of the SISO and MIMO controllers experimentally, the designed continuous-time controllers are discretized using the Bilinear transformation with a sampling frequency of $20kHz$. The discrete-time controllers

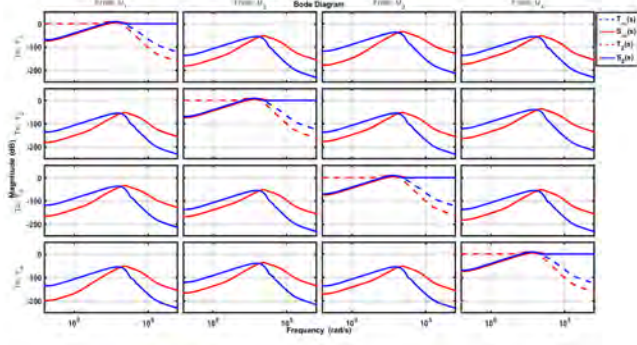


Fig. 10. Singular values of the closed-loop sensitivity functions $S(s)$ and the complementary sensitivity functions $T(s)$ using the MIMO H_2 and H_∞ optimal controllers

are implemented in real-time using an ADC/DAC converter and the dSPACE DS1104 digital signal processing board. In the first part of the experiment, the performance of the designed controllers is evaluated while the rotor is stationary and in the presence of constant disturbances. In order to investigate the disturbance rejection properties of the controllers, four unit-step disturbances are introduced to the system. The first disturbance is added to the channel 1 at approximately one second, followed by the second disturbance to the channel 2 after two seconds. The other two disturbances are introduced to the channels 3 and 4 after three and four seconds, respectively. For a fair comparison, the performance of the SISO and MIMO controllers are compared separately. The results from the SISO controllers, namely, the SISO H_∞ controllers, the lead-lag type compensators, and the analog on-board controllers are depicted in Figs. 11 and 12. Note that the analog on-board controllers are in the form of lead compensators with first-order low-pass filters and with the transfer functions of:

$$K_{on-board\ controllers(1-4)} = \frac{1.7218 \times 10^5 (s + 1128)}{(s + 3030)(s + 4.545 \times 10^4)} \quad (42)$$

It is clear from the results in Fig. 11 that the SISO H_∞ controllers certainly outperform the analog on-board controllers. On the other hand, a relatively similar performance can be achieved by the carefully designed lead-lag type compensators. However, the controller design based on the classical methods could become cumbersome if the order of the system being controlled is high. In contrast to the classical methods, the H_∞ synthesis procedure include the required components (compensators, notch filters, and the high-frequency low-pass filters) automatically if the weighting functions are chosen properly.

The performance of the MIMO H_2 and H_∞ optimal controllers are also depicted in Figs. 13 and 14. Similar behavior in terms of transient- and steady-state response can be seen from the two controllers in Fig. 13. However, from the control signals in Fig. 14, it can be deduced that the high-frequency measurement noises are much better attenuated by the H_2 controllers compare to the H_∞ controllers.

The AMB system under study consists of an internal air turbine attached to one end of the rotor that allows the

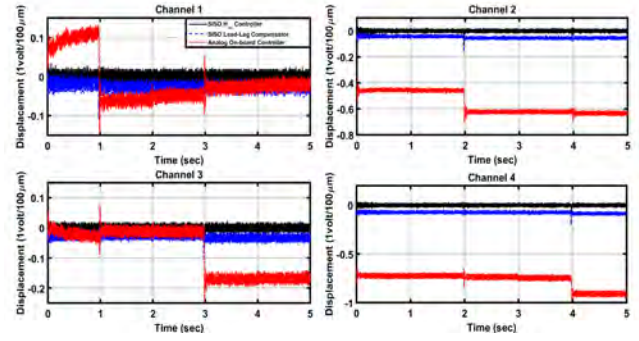


Fig. 11. Step responses of all four channels using the SISO controllers in the presence of disturbances.

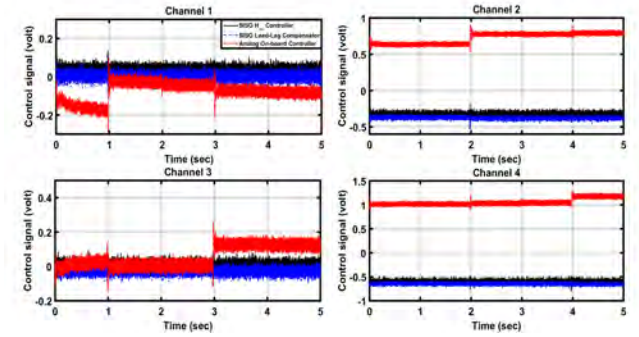


Fig. 12. Control signals of all four channels using the SISO controllers in the presence of disturbances on all four channels.

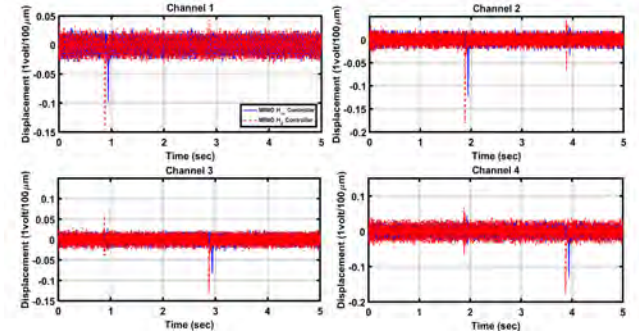


Fig. 13. Step responses of all four channels using the MIMO controllers in the presence of disturbances.

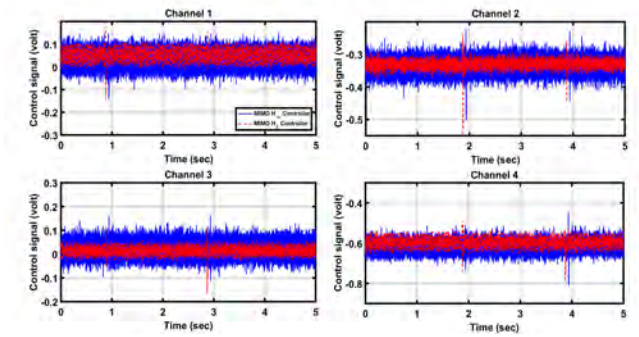


Fig. 14. Control signals of all four channels using the MIMO controllers in the presence of disturbances.

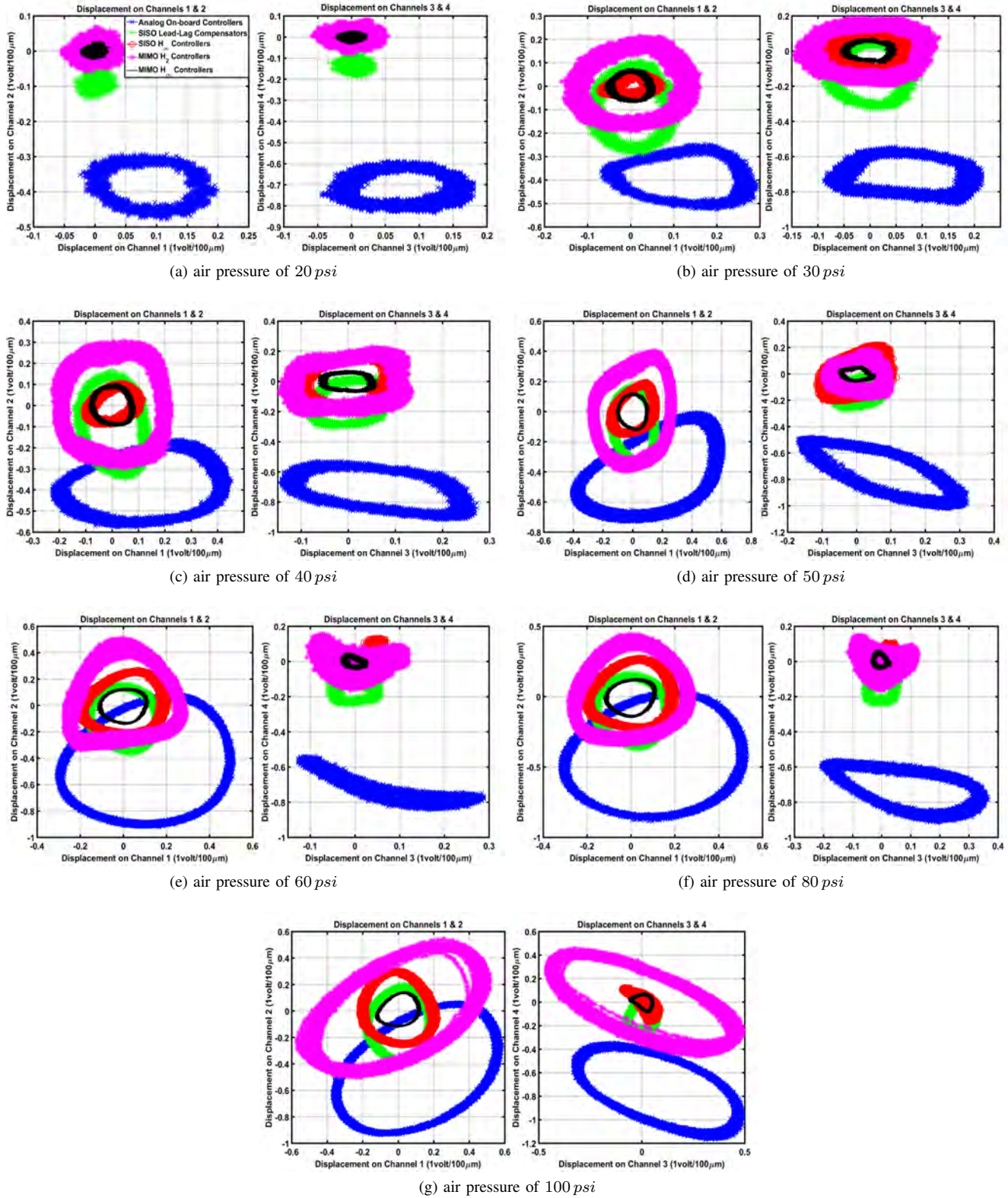


Fig. 15. Trajectory of the geometrical center of the rotor (at both ends) using the SISO and MIMO controllers.

spinning of the rotor up to 10000 *rpm*. In order to evaluate the performance of the SISO and MIMO controllers while the rotor is in rotation, the air pressure supplied by the air compressor is increased gradually, and the displacement of the

geometrical center of the rotor at both ends of the rotor are captured. The displacements of the rotor at all four channels are depicted in Fig. 15. As the rotational speed of the rotor increases, it can be seen that the overall performance of the

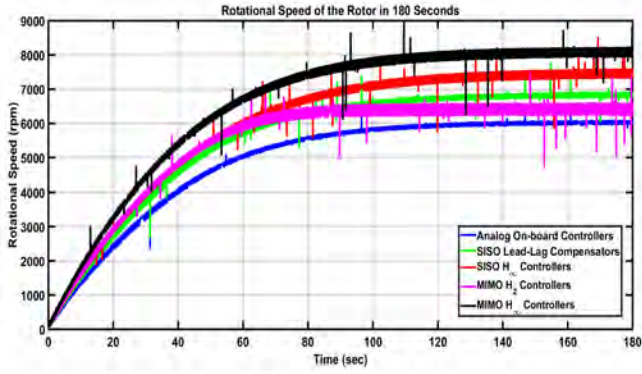


Fig. 16. Rotational speed of the rotor using the SISO and MIMO controllers.

MIMO H_∞ controller remain significantly better than all other controllers. Furthermore, unlike the stationary case, the MIMO H_2 controller shows a very poor performance compared to the MIMO H_∞ controller at high rotational speeds. Finally, the SISO H_∞ controllers show a convincing performance compared to the lead-lag-type compensators and the analog on-board controllers.

More interestingly, the rotor achieves different steady-state rotational speeds using the designed controllers while constant air pressure (100 *psi*) is supplied to the system. The transient speed responses of the system using the designed controllers are depicted in Fig. 16. The highest steady-state speed is achieved by using the MIMO H_∞ controller. This is because the effects caused by the rotor mass-imbalance and centrifugal forces are better rejected by the MIMO H_∞ controller, allowing the rotor to obtain higher rotational speeds compared to the other controllers. As it is expected, the system achieves very low steady-state speed by the MIMO H_2 controller due to the poor performance of the H_2 controllers at high rotational speeds. Furthermore, the SISO H_∞ controllers show better performance amongst the other SISO controllers. Last but not least, it can be deduced from the results that the high-order H_∞ controllers show better performance compared to the low-order H_∞ controllers. However, the price to pay is to implement excessively high-order controllers that demand more powerful hardware for a successful real-time implementation.

VI. CONCLUSION

This paper dealt with the modeling and high-performance controller design of an active magnetic bearing system. First, GA-WLS algorithm was presented to obtain the best SISO and MIMO models of the system. Next, SISO and MIMO controllers were designed on the basis of the identified models of the system. The designed controllers were discretized and implemented on the AMB system for real-time experimental analysis. The performance of the designed controllers was examined while the rotor was stationary, as well as while it was operating at several rotational speeds. All the designed controllers showed much superior performances compared to the analog on-board controllers. Moreover, it was shown that the performance of the MIMO H_2 controller was not

satisfactory at high speeds where the modeling uncertainties were more significant. Although the performance of the system was further improved by using the MIMO H_∞ controller over the SISO H_∞ controllers, but the price to pay was to implement excessively high-order controller that demanded more powerful hardware. Furthermore, it was shown that the proper modeling of the system would lead to the design of several high-performance *stable* controllers that could successfully be implemented on the system without any further modifications.

APPENDIX

A. The eighteenth-order MIMO model of the AMB system

$$A = \text{diag} \left\{ \begin{pmatrix} -0.0359 & 12900 \\ -12900 & -0.0359 \end{pmatrix}, \begin{pmatrix} -0.55 & 4826 \\ -4826 & -0.55 \end{pmatrix}, \begin{pmatrix} -0.69 & 4835 \\ -4835 & -0.69 \end{pmatrix}, \begin{pmatrix} -152 & 335.8 \\ -335.8 & -152.9 \end{pmatrix}, \begin{pmatrix} -120.9 & 341.8 \\ -341.8 & -120.9 \end{pmatrix}, \begin{pmatrix} -111.8 & 228.2 \\ -228.2 & -111.8 \end{pmatrix}, \begin{pmatrix} -70.51 & 212.4 \\ -212.4 & -70.51 \end{pmatrix}, 191.4, 243.4, 272.4, 284.5 \right\}$$

$$B = \begin{pmatrix} -0.0243 & 0.0176 & -0.0235 & -0.0193 \\ 0.0453 & -0.0672 & 0.0486 & 0.0839 \\ 0.5450 & 0.0348 & -0.5991 & 0.0686 \\ -1.4730 & 0.2672 & 1.7560 & 0.3069 \\ -0.1713 & -1.4250 & 0.2059 & -1.7710 \\ 0.0820 & -0.7334 & -0.0522 & -0.8909 \\ -5.2730 & 4.2650 & -4.8140 & -3.4230 \\ -1.7190 & -3.8070 & 3.0520 & 9.5530 \\ -5.1950 & 2.4130 & -8.4050 & -3.1360 \\ -1.4100 & 1.6070 & 1.4170 & -3.6310 \\ -2.0850 & -1.2980 & -0.3873 & 4.2370 \\ -2.0320 & 5.3700 & -1.7270 & 5.5080 \\ 7.4800 & -0.7283 & -5.0160 & -1.0070 \\ 1.1000 & 0.9193 & 1.7110 & 1.5220 \\ 8.7810 & -21.0600 & 0.5281 & 33.6300 \\ -44.7700 & -16.0000 & -53.4300 & 1.0640 \\ -50.9400 & -8.0200 & 65.9800 & 13.8900 \\ 34.1700 & -55.9100 & -50.3000 & -44.6800 \end{pmatrix}$$

$$C^T = \begin{pmatrix} -7.2300 & -2.1590 & -1.5950 & 6.9340 \\ -5.5360 & 16.7600 & -18.1900 & -20.8700 \\ -10.4100 & 0.5644 & 16.4900 & 1.6760 \\ -5.5310 & 1.7130 & 3.7640 & 1.2470 \\ -1.2190 & -6.6440 & 1.9040 & -1.9720 \\ 0.7982 & 11.4200 & -1.7800 & 14.4700 \\ -1.3220 & -15.4500 & 0.3159 & 9.0980 \\ 6.2330 & 9.8390 & 4.5670 & -3.8710 \\ 12.8700 & 16.3700 & 9.2420 & -3.2940 \\ 8.9640 & -0.9097 & 3.0000 & 1.0810 \\ 3.3940 & 1.7800 & 1.0590 & -15.4300 \\ -3.4690 & -17.5500 & 3.2230 & -10.5200 \\ -8.5000 & -1.9170 & 10.1500 & -1.3500 \\ 4.0930 & -2.0230 & -8.2030 & -2.2680 \\ 0.6677 & -2.5790 & 0.3406 & 3.1050 \\ -2.1520 & -0.2261 & -1.9370 & 0.4813 \\ -1.1260 & -1.9160 & 1.4620 & -0.5211 \\ 0.6849 & -1.9850 & 0.2637 & -1.0290 \end{pmatrix}$$

REFERENCES

- [1] J. Kumbennuss, C. Jian, J. Wang, H. X. Yang, and W. N. Fu, "A novel magnetic levitated bearing system for vertical axis wind turbines (VAWT)", *Applied Energy*, vol. 90, no. 1, pp. 148-153, 2012.
- [2] J. X. Shen, K. J. Tseng, D. M. Vilathgamuwa, and W. K. Chan, "A novel compact PMSM with magnetic bearing for artificial heart application", *IEEE Transactions on Industry Applications*, vol. 36, no. 4, pp. 1061-1068, 2000.
- [3] J. Shi, and W. S. Lee, "An experimental comparison of a model based controller and a fuzzy logic controller for magnetic bearing system stabilization", in the *Proceedings of the 7th IEEE International Conference on Control & Automation*, New Zealand, pp. 379-384, 2009.
- [4] J. Shi, and W. S. Lee, "Design and implementation of conventional and advanced controllers for magnetic bearing system stabilization", *Magnetic Bearings, Theory and Applications*, Bostjan Polajzer (Ed.), 2010.
- [5] T. Tezuka, N. Kurita, and T. Ishikawa, "Design and simulation of a five degrees of freedom active control magnetic levitated motor", *IEEE Transactions on Magnetics*, vol. 49, no. 5, pp. 2257-2262, 2013.
- [6] S. Y. Yoon, Z. L. Lin, and P. E. Allaire, "Experimental evaluation of a surge controller for an AMB supported compressor in the presence of piping acoustics", *IEEE Transactions on Control Systems Technology*, vol. 22, no. 3, pp. 1215-1223, 2014.
- [7] N. J. M. van Dijk, N. van de Wouw, E. J. J. Doppenberg, H. A. J. Oosterling, and H. Nijmeijer, "Robust active chatter control in the high-speed milling process", *IEEE Transactions on Control Systems Technology*, vol. 20, no. 4, pp. 901-917, 2012.
- [8] B. C. Han, S. Q. Zheng, X. Wang, and Q. Yuan, "Integral design and analysis of passive magnetic bearing and active radial magnetic bearing for agile satellite application", *IEEE Transactions on Magnetics*, vol. 48, no. 6, pp. 1959-1966, 2012.
- [9] X. Su, X. Yang, P. Shi, and L. Wu, "Fuzzy control of nonlinear electromagnetic suspension systems", *Mechatronics*, vol. 24, no. 4, pp. 328-335, 2014.
- [10] P. Shi, Y. Yin, F. Liu, and J. Zhang, "Robust control on saturated Markov jump systems with missing information", *Information Sciences*, vol. 265, pp. 123-138, 2014.
- [11] X. Zhao, L. Zhang, P. Shi, and H. Karimi, "Robust control of continuous-time systems with state-dependent uncertainties and its application to electronic circuits", *IEEE Transactions on Industrial Electronics*, vol. 61, no. 8, pp. 4161-4170, 2014.
- [12] M. Liu, L. Zhang, P. Shi, and H. Karimi, "Robust control for stochastic system against bounded disturbances with application to flight control", *IEEE Transactions on Industrial Electronics*, vol. 61, no. 3, pp. 1504-1515, 2014.
- [13] D. H. Lee, J. B. Park, Y. H. Joo, K. C. Lin, and C. H. Ham, "Robust H_∞ control for uncertain nonlinear active magnetic bearing systems via Takagi-Sugeno fuzzy models", *International Journal of Control, Automation and Systems*, vol. 8, no. 3, pp. 636-646, 2010.
- [14] H. Kang, S. Oh, and O. Song, " H_∞ control of a rotor-magnetic bearing system based on linear matrix inequalities", *Journal of Vibration and Control*, vol. 17, no. 2, pp. 291-300, 2011.
- [15] I. S. Kuseyri, "Robust control and unbalance compensation of rotor/active magnetic bearing systems", *Journal of Vibration and Control*, vol. 18, no. 6, pp. 817-832, 2011.
- [16] G. Barbaraci, and G. Virzi" Mariotti, "Performances comparison for a rotating shaft suspended by 4-axis radial active magnetic bearings via μ -synthesis, loop-shaping design, and sub H_∞ with uncertainties", *Modelling and Simulation in Engineering*, vol. 2011, pp. 1-10, 2011.
- [17] J. Chen, K. Liu, and K. Xiao, " H_∞ control of active magnetic bearings using closed loop identification model", in the *Proceedings of International Conference on Mechatronics and Automation*, pp. 349-353, 2011.
- [18] Z. Gosiewski and A. Mystkowski, "Robust control of active magnetic suspension: analytical and experimental results", *Mechanical Systems and Signal Processing*, vol. 22, no. 6, pp. 1297-1303, 2008.
- [19] R. P. Jastrzebski, K. M. Hynynen, and A. Smirnov, " H_∞ control of active magnetic suspension", *Mechanical Systems and Signal Processing*, vol. 24, pp. 995-1006, 2010.
- [20] R. P. Jastrzebski, A. Smirnov, O. Pyrhönen, and A. K. Piłat, "Discussion on robust control applied to active magnetic bearing rotor system", in *Challenges and Paradigms in Applied Robust Control*, ed: InTech, 2011.
- [21] H. M. N. K. Balini, C. W. Scherer, and J. Witte, "Performance enhancement for AMB systems using unstable H_∞ controllers", *IEEE Transactions on Control Systems Technology*, vol. 19, no. 6, pp.1479-1492, 2011.
- [22] H. M. N. K. Balini, J. Witte, and C. W. Scherer, "Synthesis and implementation of gain-scheduling and LPV controllers for an AMB system", *Automatica*, vol. 48, no. 3, pp. 521-527, 2012.
- [23] A. Noshadi, J. Shi, W. S. Lee, P. Shi, A. Kalam, "Optimal PID-type fuzzy logic controller for a multi-input multi-output active magnetic bearing system", *Neural Computing and Applications*, doi: 10.1007/s00521-015-1996-7, 2015.
- [24] A. Noshadi, J. Shi, W. S. Lee, P. Shi, A. Kalam, "Robust control of an active magnetic bearing system using H_∞ and disturbance observer-based control", *Journal of Vibration and Control*, doi: 10.1177/1077546315602421, 2015.
- [25] A. Noshadi, W. S. Lee, J. Shi, P. Shi, A. Kalam, "On Two-Step Controller Design for Partially Unknown Unstable Systems", in the *Proceedings of European Control Conference*, pp. 485-490, 2015.
- [26] A. Noshadi, J. Shi, W. S. Lee, P. Shi, A. Kalam, "Repetitive Disturbance Observer-based Control for an Active Magnetic Bearing System", to appear in the *Proceedings of Australian Control Conference*, 2015.
- [27] J. Doyle, B. Francis, and A. Tannenbaum, *Feedback Control Theory*, Macmillan Publishing Co., 1990.
- [28] B. A. Francis, "A course in H_∞ control theory", *Lecture Notes in Control and Information Sciences*, 1987.
- [29] W. Sun and H. Gao and B. Yao, "Adaptive Robust Vibration Control of Full-Car Active Suspensions With Electrohydraulic Actuators", *IEEE Transactions on Control Systems Technology*, vol. 21, no. 6, pp. 2417-2422, 2013.
- [30] J. Yao and Z. Jiao and D. Ma and L. Yan, "High-Accuracy Tracking Control of Hydraulic Rotary Actuators With Modeling Uncertainties", *IEEE/ASME Transactions on Mechatronics*, vol. 19, no. 2, pp. 633-641, 2014.
- [31] DS1104 R&D controller board cost-effective system for controller development, 2009, from <http://www.dspace.com>.
- [32] G. Baselli and P. Bolzern, "Closed-loop system identification", in *Wiley Encyclopedia of Biomedical Engineering*, John Wiley & Sons, Inc., 2006.
- [33] A. Noshadi, J. Shi, W. S. Lee, P. Shi, and A. Kalam, "Genetic algorithm-based system identification of active magnetic bearing system: a frequency-domain approach", in the *Proceedings of the 11th IEEE International Conference on Control & Automation*, pp. 1281-1286, 2014.
- [34] K. A. Michalski, "On the low-order partial-fraction fitting of dielectric functions at optical wavelengths", *IEEE Transactions on Antennas and Propagation*, vol. 61, no. 12, pp. 6128-6135, 2013.
- [35] Y. Todo, and T. Mitsui, "A Learning Multiple-Valued Logic Network Using Genetic Algorithm", *International Journal of Innovative Computing, Information and Control*, vol. 10, no. 2, pp. 565-574, 2014.
- [36] A. I. Al-Odienat, "The PID Controller Based on Genetic Algorithm for Voltage Stability of the Synchronous Machine", *International Journal of Innovative Computing, Information and Control*, vol. 10, no. 6, pp. 2263-2276, 2014.
- [37] J. Yang, H. Gao, and W. Liu, "Hybrid Method of Chaotic Genetic Algorithm and Boundary Simulation for Constrained Optimization", *International Journal of Innovative Computing, Information and Control*, vol. 11, no. 3, pp. 1059-1073, 2015.
- [38] A. Zolfagharian, A. Noshadi, M. R. Khosravani, and M. Z. Md Zain, "Unwanted noise and vibration control using finite element analysis and artificial intelligence", *Applied Mathematical Modelling*, vol. 38, no. 9-10, pp. 2435-2453, 2014.
- [39] K. Zhou, and J. C. Doyle, *Essentials of Robust Control*, Prentice Hall, 1999.
- [40] S. Skogestad, and I. Postlethwaite, *Multivariable Feedback Control: Analysis and Design*, vol. 2, Wiley New York, 2007.
- [41] A. Noshadi, J. Shi, W. S. Lee, P. Shi, and A. Kalam, "High performance H_∞ control of non-minimum phase active magnetic bearing system", in the *Proceedings of the 40th Annual Conference of the IEEE Industrial Electronics Society*, pp. 183-189, 2014.
- [42] J. Doyle, K. Glover, P. P. Khargonekar, and B. A. Francis, "State-space solutions to standard H_2 and H_∞ control problems", *IEEE Transactions on Automatic Control*, vol. 34, no. 8, pp. 831-847, 1989.



robots, and system identification and control of active magnetic bearing systems.

Amin Noshadi (M'12) received his Bachelor of Engineering degree from Ferdowsi University of Mashhad, Iran, in 2007 and the Master of Engineering degree from University Technology of Malaysia, in 2011. He is currently pursuing his Ph.D. degree in Electrical and Electronics Engineering in the College of Engineering and Science, Victoria University, Melbourne, Australia. His research interests include modeling and system identification of complex systems, robust control, intelligent control and applications, nonlinear control, optimization, parallel



applications, smart energy systems, system identification, and engineering education.

Juan Shi (M'91) received her honorary Bachelor of Engineering degree from Northeastern University, China, in 1988 and the Ph.D. degree in Electrical Engineering from Victoria University (VU), Melbourne, Australia, in 1995. Dr Shi obtained her Graduate Certificate in Tertiary Education from VU in 2003. She joined VU as a lecturer in 1994 and she is currently a Senior Lecturer in the College of Engineering & Science at VU. Her current research interests include power system stability, automatic control and applications, fuzzy logic control and



He enjoys teaching and solving problems in control, communications and signal processing. His current research interests are in signal processing and its application to control, communications and biomedical engineering.

Wee Sit Lee received the B.Eng. degree and the M.Sc. degree in electrical engineering from the National University of Singapore. He joined Victoria University in Melbourne, Australia, as a Senior Lecturer after receiving a Ph.D. degree in systems engineering from the Australian National University.



He was actively served in the editorial board of a number of journals, including *Automatica*, *IEEE Transactions on Automatic Control*; *IEEE Transactions on Fuzzy Systems*; *IEEE Transactions on Cybernetics*; *IEEE Transactions on Circuits and Systems-I: Regular Papers*; and *IEEE Access*. He is a Fellow of the Institute of Electrical and Electronic Engineers, the Institution of Engineering and Technology, and the Institute of Mathematics and its Applications.

Peng Shi (M'95/SM'98/F'15) received the B.Sc. degree in Mathematics from Harbin Institute of Technology, China; the M.Eng. degree in Systems Engineering from Harbin Engineering University, China; the Ph.D. degree in Electrical Engineering from the University of Newcastle, Australia; the PhD degree in Mathematics from the University of South Australia. He was awarded the Doctor of Science degree from the University of Glamorgan, UK in 2006, and the Doctor of Engineering degree from the University of Adelaide, Australia in 2015. Dr Shi is



smart grid, IEC61850 implementation and cogeneration systems. He has been actively engaged in the teaching of Energy Systems to undergraduates, postgraduates and providing professional courses to the industry both in Australia and overseas. He regularly offers Continuing Professional Development and Master Class courses on Power System Protection, Renewable Energy, IEC61850, Cogeneration & Gas Turbine Operation and PBL in engineering education to practicing engineers, the Energy Supply Association of Australia (ESAA), and Australian Power Institute (API). He also runs postgraduate distance education programme on Power System Protection for the ESAA. He has conducted research, provided industrial consultancy and published over four hundred and seventy publications on his area of expertise and written over 29 books in the area. Professor Kalam is a Fellow of EA, IET, AIE, a member of IEEE and CIGRE AP B5.

Akhtar Kalam has been at Victoria University, Melbourne since 1985 and a former Deputy Dean of the Faculty of Health, Engineering and Science for 7 years. He is currently the Discipline Group Leader of Electrical, Electronic and Sports Engineering. He has wide experience in educational institutions and industry across four continents. He is regularly invited to deliver lectures, work on industrial projects and examine external thesis overseas. His major areas of interests are power system analysis, communication, control, protection, renewable energy,